The curvature of material surfaces in isotropic turbulence

S. B. Pope, P. K. Yeung,[a] and S. S. Girimaji
Sibley School of Mechanical and Aerospace Engineering, Cornell University, Ithaca, New York 14853

(Received 3 May 1989; accepted 10 August 1989)

Direct numerical simulation is used to study the curvature of material surfaces in isotropic turbulence. The Navier–Stokes equation is solved by a 64^3 pseudospectral code for constant-density homogeneous isotropic turbulence, which is made statistically stationary by low-wavenumber forcing. The Taylor-scale Reynolds number is 39. An ensemble of 8192 infinitesimal material surface elements is tracked through the turbulence. For each element, a set of exact ordinary differential equations is integrated in time to determine, primarily, the two principal curvatures k_1 and k_2. Statistics are then deduced of the mean-square curvature $M = \frac{1}{2}(k_1^2 + k_2^2)$, and of the mean radius of curvature $R = (k_1^2 + k_2^2)^{-1/2}$. Curvature statistics attain an essentially stationary state after about 15 Kolmogorov time scales. Then the area-weighted expectation of R is found to be 12η, where η is the Kolmogorov length scale. For moderate and small radii (less than 10η) the probability density function (pdf) of R is approximately uniform, there being about 5% probability of R being less than η. The uniformity of the pdf of R, for small R, implies that the expectation of M is infinite. It is found that the surface elements with large curvatures are nearly cylindrical in shape (i.e., $|k_1| \gg |k_2|$ or $|k_2| \gg |k_1|$), consistent with the folding of the surface along nearly straight lines. Nevertheless the variance of the Gauss curvature $K = k_1 k_2$ is infinite.

I. INTRODUCTION

In the study of mixing[1,2] and reaction[3] in turbulent flows, there are several phenomena that can be usefully described in terms of surfaces. For example, in the flamelet regime of turbulent combustion,[4] reaction is confined to the flame sheet—a surface that can be highly wrinkled and possibly disconnected.

Three types of surfaces have been considered. The most basic, and that studied here, is the material surface. By definition, a material surface moves with the fluid: every point of the surface is a fluid particle. For premixed combustion (in the flamelet regime) the flame sheet is a propagating surface: each point on the surface moves (relative to the fluid) at the local flame speed in the direction normal to the surface. For nonpremixed reaction, the reaction sheet is a constant-property surface: at each point on the surface the mixture is stoichiometric. In the appropriate limits (vanishing flame speed or diffusivity) both propagating surfaces and constant-property surfaces become material surfaces.

We consider an infinite, initially plane material surface in statistically stationary, constant-density, homogeneous, isotropic turbulence. As time evolves, the turbulence convects, stretches, and bends the surface. Material-surface stretching has been considered theoretically by Batchelor,[1,2] Cocke,[5] and Orszag.[6] In a recent study,[7] we have used direct numerical simulations (DNS) of isotropic turbulence to quantify the statistics of material-surface stretching.

As the surface is stretched and bent, its topology does not change.[8] The surface cannot intersect itself; holes are not created; and a singularity (infinite curvature) cannot develop in finite time. (These results depend on the assumption that the second spatial derivative of the velocity field is bounded.)

To provide a complete statistical description of the geometry of the surface is a massive task—as it is to provide a complete description of a turbulent velocity field. As in the latter case, a natural starting point for providing a partial description is the study of single-point statistics. At each point on the surface the local geometry is described by the two principal curvatures k_1 and k_2 ($k_1 \geqslant k_2$) and by the orientation of the surface.[8,9] In isotropic turbulence, the orientation of the surface is statistically isotropic and independent of the curvatures. Consequently, the joint probability density function of k_1 and k_2 provides a complete one-point statistical description of the local geometry of the surface. In this work the joint pdf of k_1 and k_2 is determined from a direct numerical simulation, and various statistics deduced from it are presented.

The distribution of curvatures provides, of course, only a partial description of the statistical geometry of the surface. There has been considerable interest[10,11] in the fractal nature of surfaces in turbulence. Since curvatures describe the surface only on an infinitesimal scale, they contain no fractal information.

Little has hitherto been known about the curvature of material surfaces. Pope[8] derived ordinary differential equations for k_1 and k_2, which show that the second spatial derivative of the fluid velocity causes the surface to bend. The curvature thus generated can be amplified (or attenuated) and reorientated by the straining of the fluid. An open question is whether the curvature, characterized by the mean-square curvature

$$M \equiv \tfrac{1}{2}(k_1^2 + k_2^2), \tag{1}$$

remains bounded, or whether as a result of straining it in-

[a] Current address: Mechanical Engineering, Queen's University, Kingston, Ontario K7L 3N6, Canada.

 0899-8213/89/122010-09$01.90

creases (presumably exponentially) with time. It has been shown[8] that if straining is uncorrelated with the orientation of the curvature then strain causes M to decrease; while on the other hand persistent straining can cause exponential growth. In fact, since M is a random variable, the question needs to be stated more precisely. And our results produce a somewhat subtle answer: the distribution of M becomes essentially stationary, even though its mean $\langle M \rangle$ increases exponentially with time.

In the next section we describe the direct numerical simulation performed to generate the velocity field $\mathbf{U}(\mathbf{x},t)$. The Navier–Stokes equation is solved on a $(64)^3$ grid, for isotropic turbulence (made stationary by low-wavenumber forcing). The Taylor-scale Reynolds number is $R_\lambda = 39$.

The method of determining material surface curvature statistics is described in Sec. III. A large number ($I = 8192$) of infinitesimal surface elements[8] are considered, each with its own position $\mathbf{X}(t)$, infinitesimal area $dA(t)$, unit normal vector $\mathbf{N}(t)$, principal curvatures $k_1(t), k_2(t)$ and principal directions $e_1^*(t), e_2^*(t)$. For each element these properties evolve in time according to a set of exact ordinary differential equations.[8] These equations contain the velocity and its first two spatial derivatives following the surface element, which are obtained from the direct numerical simulation. The resulting $I = 8192$ time series of $k_1(t)$, $k_2(t)$, etc. are used to estimate statistics such as the joint pdf of k_1 and k_2.

For the present purposes, the above method (based on infinitesimal surface elements) has distinct advantages. An alternative approach would be to represent the whole surface discretely in terms of I nodes (i.e., fluid particles), which are tracked. Another approach[12,13] is to identify the material surface with a constant-property surface of a nondiffusive convected scalar $G(\mathbf{x},t)$. [That is, the surface is the set of points $\mathbf{X}(t)$ for which $G(\mathbf{X}(t),t) = 0$.] The convection equation is then solved for $G(\mathbf{x},t)$ numerically. Both of these approaches have the disadvantage that the whole surface has to be represented, and resolved, numerically. Since the surface area increases exponentially on the Kolmogorov time scale, and since radii of curvatures less than a millionth of the Kolmogorov length scale are experienced, the demands of resolution soon exhaust any computer's capabilities.

In the present approach representative surface elements, rather than the whole surface, are described numerically. And the curvatures are computed by solving ordinary differential equations, not by differentiating the surface. Consequently, while the velocity field must be well resolved, elements with radii of curvature far less than the grid spacing can be tracked without significant numerical error.

The results of the simulation are presented in Sec. IV, and conclusions are drawn in the final section.

II. DIRECT NUMERICAL SIMULATION

A modified version of Rogallo's pseudospectral code[14] is used to solve the Navier–Stokes equation in a cubic domain with periodic boundary conditions. Low-wavenumber forcing, similar to that of Eswaran and Pope,[15] is used to add energy, so that the turbulence is stationary in spite of viscous decay. A 64^3 grid is used (with uniform grid spacing Δx), and the kinematic viscosity is chosen to yield good spatial resolution. This is characterized by $k_{\max}\eta = 1.5$, where η is the Kolmogorov length scale and $k_{\max}$ is the magnitude of the largest resolved wavenumber. The resulting Taylor-scale Reynolds number is $R_\lambda = 39$. A constant time step Δt is used, corresponding to a Courant number of about $\frac{1}{2}$ or $\Delta t/\tau_\eta = 0.052$, where τ_η is the Kolmogorov time scale. The principal numerical parameters and Eulerian statistics are given in Table I. The conditions of the simulations are statistically identical to the 64^3 R_λ 38 run reported by Yeung and Pope,[16] where further details of the simulations and of the Eulerian and Lagrangian velocity statistics obtained can be found.

Prior to the release of the material surface (at $t = 0$), the velocity field is allowed to evolve for some time so that at $t = 0$ the turbulence is statistically stationary. Then, from $t = 0$, a total of 2000 time steps are taken to reach the final time $t = T \approx 104\tau_\eta$.

At $t = 0$ a total of $I = 8192$ fluid particles are positioned on the nodes of two uniform $(16)^3$ meshes (of spacing $4\,\Delta x$), displaced relative to each other by $2\,\Delta x$ in each direction. The fluid particles are tracked using the algorithm of Yeung and Pope,[17] in which the velocities of the fluid particles are obtained by cubic-spline interpolation.

In order to integrate the surface curvature equations, the first and second spatial derivatives of velocity are required at the fluid particle locations. The nine first derivatives are formed in wavenumber space and transformed into physical space. Cubic splines are then fitted to these first derivatives; and second derivatives are obtained by differentiating the splines. (It is found that the alternative practice of differentiating the splines of velocity twice to obtain the second derivatives introduces unacceptable numerical errors.)

III. SURFACE ELEMENT PROPERTIES

A. Definitions and evolution equations

The definitions, properties, and equations for infinitesimal surface elements are given by Pope.[8] Here, for completeness, the essential results are given.

The location of each surface point considered is defined by its initial value $\mathbf{X}(0)$, and by the fact that it moves with the fluid:

TABLE I. Numerical parameters and Eulerian statistics.

Grid size	N	64
Length of solution domain	L_0	2π
Kinematic viscosity	ν	0.025
Turbulence intensity	u'	1.60
Dissipation rate	$\langle\epsilon\rangle$	2.69
Longitudinal integral length scale $\mathscr{L}_1$	$\mathscr{L}_1/(\frac{1}{2}\mathscr{L}_0)$	0.369
Dissipation time scale $\tau_\epsilon = \frac{3}{2}u'^2/\langle\epsilon\rangle$	τ_ϵ	1.43
Eddy turnover time $T_e = \mathscr{L}_1/u'$	T_e/τ_ϵ	0.507
Kolmogorov time scale τ_η	τ_η/τ_ϵ	0.067
Duration of simulation T	T/T_e	13.8
	T/τ_η	104.
Time step Δt	$\Delta t/\tau_\eta$	0.052
Kolmogorov length scale η	$\eta/\mathscr{L}_1$	0.042
Maximum resolved wavenumber $k_{\max}$	$k_{\max}\eta$	1.48
Taylor microscale λ	$\lambda/\mathscr{L}_1$	0.521
Taylor-scale Reynolds number	R_λ	38.7

$$\frac{d}{dt}\mathbf{X}(t) = \mathbf{U}(\mathbf{X}[t],t). \tag{2}$$

For each element, a time-dependent Cartesian coordinate system is introduced, with its origin at $\mathbf{X}(t)$, and with orthonormal basis vectors $\mathbf{e}_i(t)$ $(i = 1,2,3)$. The unit vector $\mathbf{e}_3(t)$ is coincident with the normal, i.e.,

$$\mathbf{e}_3(t) = \mathbf{N}(t), \tag{3}$$

and consequently $\mathbf{e}_1(t)$ and $\mathbf{e}_2(t)$ are in the tangent plane of the surface at $\mathbf{X}(t)$. Initially $(t = 0)\mathbf{e}_1(0)$ is specified arbitrarily in the tangent plane and $\mathbf{e}_2(0)$ is determined by orthogonality. Subsequently, $\mathbf{e}_1(t)$ and $\mathbf{e}_2(t)$ rotate with the fluid. These specifications lead[8] to the following evolution equations:

$$\frac{d}{dt}\mathbf{e}_\alpha = \frac{1}{2}\mathbf{e}_\beta\left(\frac{\partial U_\beta}{\partial y_\alpha} - \frac{\partial U_\alpha}{\partial y_\beta}\right)^0 + e_3\left(\frac{\partial U_3}{\partial y_\alpha}\right)^0, \tag{4}$$

$$\frac{d}{dt}\mathbf{e}_3 = -\mathbf{e}_\alpha\left(\frac{\partial U_3}{\partial y_\alpha}\right)^0. \tag{5}$$

Here y_1 and y_2 are coordinates in the $\mathbf{e}_1$ and $\mathbf{e}_2$ directions; Greek suffices take the values 1 or 2; the summation convention applies; and, the superscript 0 indicates that the quantities are evaluated at the origin.

The infinitesimal area of the surface element is denoted by $dA(t)$, and the area amplification factor $A(t)$ is defined by

$$A(t) \equiv \frac{dA(t)}{dA(0)}. \tag{6}$$

Note that $A(0)$ is unity. The area increases as a result of straining, according to

$$\dot{A} = Aa, \tag{7}$$

where

$$a(t) \equiv \left(\frac{\partial U_\alpha}{\partial y_\alpha}\right)^0 \tag{8}$$

is the rate of strain in the tangent plane.

Let $h(y_1,y_2,t)$ denote the height of the surface above the tangent plane. For sufficiently small distances $r \equiv (y_\alpha y_\alpha)^{1/2}$, h is a single-valued function with bounded derivatives. Derivatives of h at the origin are denoted by, for example,

$$h^0_{\alpha\beta} \equiv \left(\frac{\partial^2 h}{\partial y_\alpha\, \partial y_\beta}\right)^0. \tag{9}$$

Since the tangency of the surface at the origin implies $h^0 = 0$ and $h^0_\alpha = 0$, a Taylor series expansion yields

$$h(y_1,y_2) = \tfrac{1}{2} y_\alpha y_\beta h^0_{\alpha\beta} + O(r^3). \tag{10}$$

That is, the geometry of the surface near the origin is described (to second order) by the symmetric, second-order, two-dimensional tensor $h^0_{\alpha\beta}(t)$.

The principal curvatures $k_1(t)$ and $k_2(t)$ are defined as the eigenvalues of $h^0_{\alpha\beta}(t)$, with the convention $k_1 \geqslant k_2$. And the corresponding eigenvectors $\mathbf{e}^*_1$ and $\mathbf{e}^*_2$ are the principal directions of curvature. With y^*_1 and y^*_2 denoting coordinates in the principal directions, Eq. (10) can also be written,

$$h(y^*_1,y^*_2) = \tfrac{1}{2} y^{*2}_1 k_1 + \tfrac{1}{2} y^{*2}_2 k_2 + O(r^3). \tag{11}$$

The evolution equation for $h^0_{\alpha\beta}(t)$ is derived by Pope.[8] For incompressible flow it is

$$\dot{h}^0_{\alpha\beta} = \left(\frac{\partial^2 U_3}{\partial y_\alpha\, \partial y_\beta}\right)^0 - a h^0_{\alpha\beta} - (s_{\gamma\beta} h^0_{\alpha\gamma} + s_{\gamma\alpha} h^0_{\beta\gamma}), \tag{12}$$

where

$$s_{\alpha\beta} \equiv \frac{1}{2}\left(\frac{\partial U_\alpha}{\partial y_\beta} + \frac{\partial U_\beta}{\partial y_\alpha}\right)^0 \tag{13}$$

is the strain-rate tensor in the tangent plane. (Note that $a = s_{\alpha\alpha}$.)

Corresponding to Eq. (12), the equation for k_1 is

$$\dot{k}_1 = \left(\frac{\partial^2 U_3}{\partial y^{*2}_1}\right)^0 - k_1\left(3\frac{\partial U^*_1}{\partial y^*_1} + \frac{\partial U^*_2}{\partial y^*_2}\right)^0, \tag{14}$$

where

$$U^*_\alpha = \mathbf{e}^*_\alpha \cdot \mathbf{U}. \tag{15}$$

A complete set of equations has now been presented for the surface properties $\mathbf{X}$, $\mathbf{N} = \mathbf{e}_3$, $\mathbf{e}_\alpha$, A, and $h^0_{\alpha\beta}$ [Eqs. (2), (4), (5), (7), and (12)], respectively. From given initial conditions, these can be integrated, given the time series of $\mathbf{U}$, $\partial U_i/\partial x_j$, and $\partial^2 U_i/\partial x_j\, \partial x_k$ following the fluid particle. Hence the curvatures k_1 and k_2 are determined as the eigenvalues of $h^0_{\alpha\beta}$.

Since the turbulence is isotropic, the initial condition $N(0)$ is arbitrary. For convenience we specify $\mathbf{e}_i(0)$ to be coincident with the axes used in the direct numerical simulation. The infinitesimal surface elements are specified to be plane initially: that is,

$$h^0_{\alpha\beta}(0) = 0. \tag{16}$$

The equations are integrated numerically by a second-order Runge–Kutta method. It is found that the time-stepping errors are negligibly small if a time step of $2\,\Delta t \sim \frac{1}{10}\tau_\eta$ is used. This practice—as opposed to using the DNS time step Δt—provides a computational saving, since the velocity derivatives and their splines need be formed only on alternate DNS time steps.

B. Determination of statistics

The integration of the surface equations yields the time series of curvature, etc. for $I = 8192$ surface elements. For a surface property $\phi(t)$, its mean over the elements $\langle\phi(t)\rangle$ can be estimated by

$$\overline{\phi(t)} \equiv \frac{1}{I}\sum_{i=1}^{I} \phi_i(t), \tag{17}$$

where $\phi_i(t)$ is the value of $\phi(t)$ for the ith element. But for most purposes, the relevant mean is the surface mean[8] $\langle\phi(t)\rangle_A$, which is area weighted. This can be estimated by

$$\overline{\phi(t)}^A \equiv \frac{1}{I}\sum_{i=1}^{I} w_i(t)\phi_i(t), \tag{18}$$

where the weights $w_i(t)$ are

$$w_i(t) = \frac{A_i(t)}{(1/I)\Sigma_{j=1}^{I} A_j(t)} = \frac{A_i(t)}{\overline{A(t)}}. \tag{19}$$

The statistical error in approximating $\langle \phi(t) \rangle_A$ by $\overline{\phi(t)}^A$ is proportional to $\sqrt{I}$ and also to the standard deviation of $\phi_i(t) w_i(t)$. As discussed at length by Yeung, Girimaji, and Pope,[7] the standard deviation of $w_i(t)$ (initially zero) grows exponentially on the Kolmogorov time scale, and consequently so does the statistical error.

For quantities that become statistically stationary (after a time t', say), this statistical error is reduced by two techniques. First, in the definition of the weights [Eq. (19)], $A_i(t)$ is replaced by $A_i(t)/A_i(t-t')$ (for $t > t'$). This corresponds to considering the surface at age t'. (The legitimacy and efficacy of this technique is fully described in Ref. 7.) Second, the statistic is time averaged from $t = t'$ to the end of the time series $t = T$.

C. Numerical accuracy

The numerical accuracy depends on the spatial resolution (indicated by $\Delta x/\eta$ being small) and on the temporal resolution (indicated by $\Delta t/\tau_\eta$ and the Courant number being small). For the Eulerian simulation, it has been demonstrated in previous studies[15-17] that good resolution is achieved with $k_{\max}\eta \approx 1.5$ (corresponding to $\Delta x/\eta \approx 2$) and $C \approx \frac{1}{2}$. However, the resolution required depends on the quantity studied. Of the quantities required to determine the surface curvature (U_i, $\partial U_i/\partial x_j$ and $\partial^2 U_i/\partial x_j\,\partial x_k$), the second derivatives impose the most stringent resolution requirements.

The resolution of the velocity gradients is examined through their spectra. With $E(k)$ being the energy spectrum function, $k^2E(k)$ and $k^4E(k)$ represent the spectra of the first and second spatial derivatives, respectively. Figure 1 shows these spectra, both for the 64^3 simulation used (solid symbols) and also for a statistically identical 128^3 simulation with twice the resolution ($k_{\max}\eta \approx 3$).

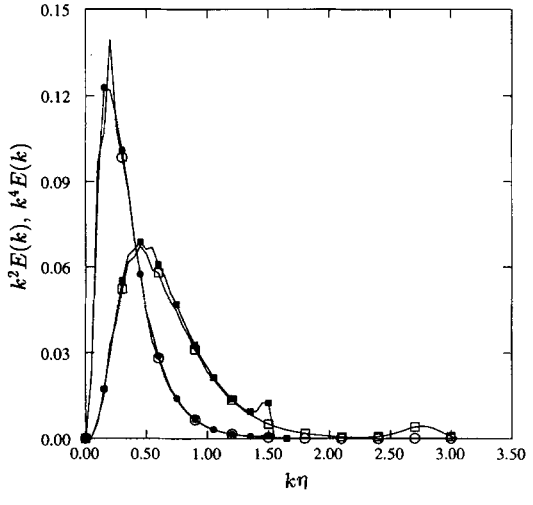

FIG. 1. Spectra of first and second spatial velocity derivatives. Circles, $k^2E(k)$; squares, $k^4E(k)$; full symbols, 64^3 simulations; open symbols, 128^3 simulations.

The peak of $k^2E(k)$ is at $k\eta \approx \frac{1}{5}$, and clearly there is negligible spectral content beyond the resolution of the 64^3 simulation (i.e., beyond $k\eta \approx 1.5$). (The small differences between the spectra from the two simulations is due to statistical variability.)

In comparison, the spectrum $k^4E(k)$ is shifted to higher wavenumbers—peaking at $k\eta \approx \frac{1}{2}$—and decays more slowly. From the 128^3 result it may be seen that $k^4E(k)$ is discernibly nonzero at $k\eta = 2$, and there is a bump centered at $k\eta = 2.75$. This is certainly a numerical artifact, due either to finite resolution or to residual aliasing errors. In any event, its contribution to the integral of $k^4E(k)$ is less than 4%. Except for a small statistical variation, the spectra $k^4E(k)$ from the two simulations are in agreement for wavenumbers up to $k\eta = 1.3$. Then there is an upturn and bump in the spectrum from the 64^3 simulation. Wavenumbers beyond $k\eta = 1.3$ make a 6% contribution to the integral of the true spectrum $k^4E(k)$ (i.e., the 128^3 spectrum excluding the bump). Therefore we take 6% as our estimate of the errors in the second derivatives as a result of finite spatial resolution.

The results show that surface radii of curvature R less than a millionth of the Kolmogorov scale η are observed. Since both $\Delta x/R$ and the Courant number based on R can be very large ($\sim 10^5$), careful consideration needs to be given to whether numerical accuracy for the radii of curvature can, nevertheless, be claimed.

The sources of numerical error in determining $k_1(t)$ and $k_2(t)$—beyond those incurred in the Eulerian simulation—are threefold. First there is the time-stepping error in integrating the surface-element ordinary differential equations. Inspection of Eq. (12) or (14) suggests that the time scale of change of k_α is no smaller than the Kolmogorov time scale τ_η: this is confirmed by the results. Hence the time step $2\,\Delta t \approx \frac{1}{10}\tau_\eta$ is sufficiently small, as tests verify.

Second, there is some error involved in interpolating for the velocity derivatives. As the tests performed by Yeung and Pope[17] show, with the current resolution ($k_{\max}\eta \approx 1.5$) and using cubic-spline interpolation, this error is less than 1%.

Third, there is a numerical error (again investigated by Yeung and Pope[17]) in the integration of Eq. (2) to determine the element location $\mathbf{X}(t)$. Given the dispersive nature of turbulence, for t large compared to τ_η, this error could be large—certainly large compared to $10^{-6}\eta$. But the error in $\mathbf{X}(t)$ can, alternatively, be viewed as a small error in the initial condition. That is, the numerically determined particle position $\mathbf{X}(t)$ is the exact position of the particle originating from $\mathbf{X}(0) + \delta\mathbf{X}$, where $|\delta\mathbf{X}|$ is small (compared to η). And the time series of the velocity gradients of the particles originating from $\mathbf{X}(0)$ and $\mathbf{X}(0) + \delta\mathbf{X}$ differ little. Since we are interested in the statistics of a statistically homogeneous surface, the precise initial condition of the surface elements considered is unimportant.

In summary, in the current method of tracking infinitesimal surface elements, good resolution of the Kolmogorov length and time scales is sufficient for the accurate calculation of surface statistics. Resolution on the scales of the surface radii of curvature is not required. This conclusion is in

marked contrast to that for other methods in which the whole surface is represented numerically.

IV. RESULTS

A. Stationarity

The results reported in subsequent subsections are statistics of the surface curvature in the statistically stationary state. The purpose of this subsection is to demonstrate that this state is achieved after about 15 Kolmogorov time scales.

For each surface element the normalized mean-square curvature is defined by

$$M^*(t) = \eta^2 M(t) = \tfrac{1}{2}\eta^2[k_1(t)^2 + k_2(t)^2], \tag{20}$$

and we define $\mathscr{L}$ as its logarithm:

$$\mathscr{L}(t) \equiv \ln M^*(t). \tag{21}$$

Figures 2 and 3 show the temporal evolution of the area-weighted mean $\langle \mathscr{L} \rangle_A$ and variance σ_A^2 of $\mathscr{L}$, which are estimated by Eqs. (18) and (19). It may be seen that stationarity is, plausibly, reached at about $t = 15\tau_\eta$: but there are large statistical fluctuations. (The statistical errors grow exponentially with time; see Sec. III. B.) Because of the statistical error, the evidence of Figs. 2 and 3 may be regarded as inconclusive. A further piece of evidence is based on the probability density function (pdf) of $\mathscr{L}$. Let $p^A(l)$ be the area-weighted pdf of $\mathscr{L}$ [i.e., $p^A(l)$ is the area-weighted probability density of the event $\mathscr{L} = l$]. The standardized random variable $\hat{\mathscr{L}}$ is defined by

$$\hat{\mathscr{L}} = (\mathscr{L} - \langle \mathscr{L} \rangle_A)/\sigma_A, \tag{22}$$

and its pdf is denoted by $\hat{p}^A(\hat{l})$, where

$$\hat{p}^A(\hat{l}) = \sigma_A p^A(l), \tag{23}$$

and the standardized sample-space variable $\hat{l}$ is

$$\hat{l} = (l - \langle \mathscr{L} \rangle_A)/\sigma_A. \tag{24}$$

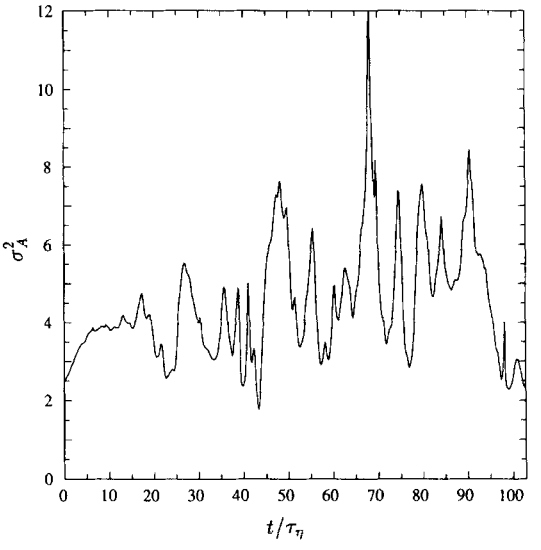

FIG. 3. Area-weighted variance of the logarithm of the normalized mean-square curvature against time normalized by the Kolmogorov time scale.

(By definition, $\hat{p}^A$ has zero mean and unit variance.)

Standardized pdf's $\hat{p}^A(\hat{l})$ are shown in Fig. 4, and the means $\langle \mathscr{L} \rangle_A$ and variances σ_A^2 are given in Table II. These are obtained by time averaging, using different surface ages t' (see Sec. III. B). A necessary and sufficient condition for stationarity is that the statistic [i.e., $\hat{p}^A(\hat{l})$] becomes independent of t' for sufficiently large t'. It may be seen from the figure that with $t'/\tau_\eta = 0$, 5.2, and 10.3, there are discernible differences compared to the pdf's with $t'/\tau_\eta = 15.5$, 20.6, and 25.8. But these latter pdf's differ among themselves only by small statistical errors. The same conclusions can be drawn from means and variances given in Table II. (Results are not reported for $t'/\tau_\eta > 25.8$ because of the large statistical errors.)

Based on this evidence, we conclude that the pdf of

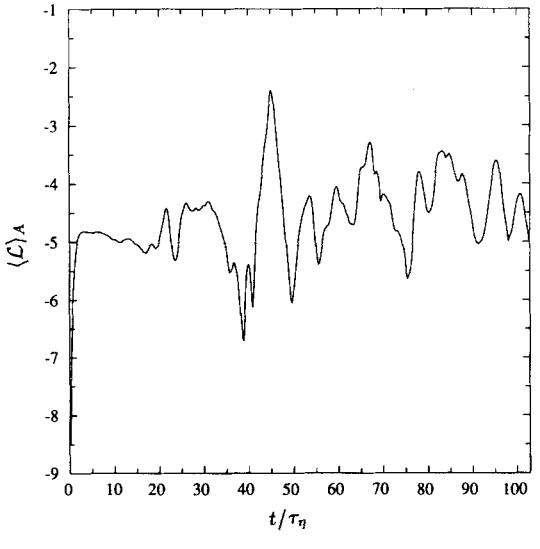

FIG. 2. Area-weighted mean of the logarithm of the normalized mean-square curvature against time normalized by the Kolmogorov time scale.

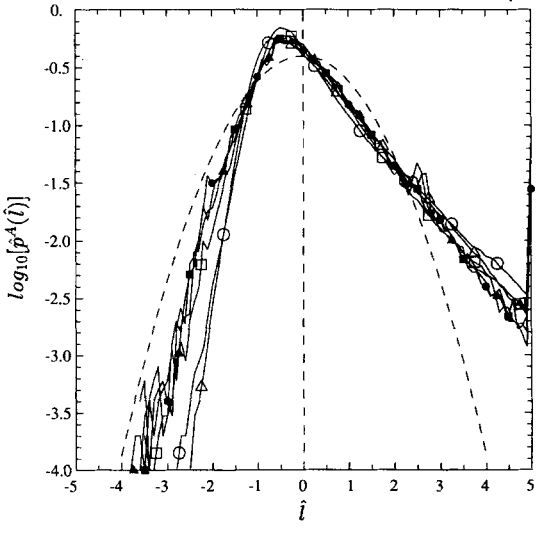

FIG. 4. Standardized area-weighted pdf's of $\mathscr{L} = \ln M^*$ for different surface ages, t'. Here $t'/\tau_\eta = 0$, △; 5.2, ○; 10.3, □; 15.5, ▲; 20.6, ●; 25.8, ■. (The dashed line corresponds to a Gaussian pdf.)

TABLE II Area-weighted mean and variance of $\mathscr{L} = \ln M^*$ for different surface ages t'.

t'/τ_η	$\langle \mathscr{L} \rangle_A$	σ_A^2
0	−2.09	16.4
5.2	−4.09	9.92
10.3	−4.66	5.82
15.5	−4.77	4.74
20.6	−4.78	4.45
25.8	−4.80	4.14

$\ln M^*$ is most likely stationary after 15 Kolmogorov time scales. The statistics presented in the following subsections are obtained by time averaging with $t' = 15.5\tau_\eta$.

B. Mean-square curvature

In this subsection we present statistics of the normalized mean-square curvature $M^*(t)$ [Eq. (20)], and of the directly related mean radius of curvature defined by

$$R^* \equiv R/\eta = 1/(\eta\sqrt{2M}) = 1/\sqrt{2M^*}. \tag{25}$$

The significance of R is that if the element is cylindrical ($k_1 > 0, k_2 = 0$; or, $k_1 = 0, k_2 < 0$) then R is the radius of curvature ($1/k_1$ or $1/|k_2|$).

We define $p_R^A(r)$ and $p_M^A(m)$ to be the area-weighted pdf's of R^* and M^*, respectively. These are related to the pdf of $\mathscr{L}$ by

$$p_R^A(r) = 2\sqrt{2}\exp(\tfrac{1}{2}l)p^A(l), \quad r = 1/\sqrt{2}\exp(-\tfrac{1}{2}l) \tag{26}$$

and

$$p_M^A(m) = e^{-l}p^A(l), \quad m = e^l. \tag{27}$$

Figure 5 shows the standardized pdf of $\mathscr{L}$, $\hat{p}^A(\hat{l})$. The mean and standard deviation of $\mathscr{L}$ are $\langle \mathscr{L} \rangle_A = -4.77$ and $\sigma_A = 2.18$: the skewness and flatness factors are 1.5 and 7.1, respectively. The dashed line on the figure is the parabola corresponding to the pdf if M^* were lognormally distributed. Clearly the lognormal distribution does not, even qualitatively, describe the shape of the pdf.

It appears from the figure that for large curvatures the pdf has the asymptotic form

$$p^A(l) \sim be^{-cl}, \tag{28}$$

with $b = 0.0172$ and $c = 0.55$. An immediate consequence of this behavior is that the expectation of the mean-square curvature is infinite. For (if the integrals converge) $\langle M^* \rangle$ is given by

$$\langle M^* \rangle = \int_0^\infty m p_M^A(m)\,dm, \tag{29}$$

or [from Eq. (27)]

$$\langle M^* \rangle = \int_{-\infty}^\infty e^l p^A(l)\,dl. \tag{30}$$

It is clear from Eq. (30) that, with the asymptotic form of Eq. (28), the integral converges only for $c > 1$—which is not the case here.

In fact, the evolution equation for k_1 [Eq. (14)] shows that k_1 (and hence M^*) can grow at most exponentially with time (assuming that the velocity gradients are bounded). As an illustration, Fig. 6 shows the time series of $\sqrt{M^*}$ for the surface element that attains the largest value of M^*. It may be seen that between $t/\tau_\eta = 49$ and $t/\tau_\eta = 57$ it experiences a rapid rise in M^*, at the approximate rate $d\mathscr{L}/dt \approx 1.8/\tau_\eta$.

The picture that emerges from these considerations is as follows. After a development time ($\approx 15\tau_\eta$), for all but very high curvatures ($\hat{\mathscr{L}} < 5$, say), the pdf of $\mathscr{L} = \ln M^*$ adopts the stationary distribution shown in Fig. 5, which has the asymptotic form Eq. (28). For larger and larger curvatures, it takes longer and longer for the pdf $p^A(l)$ to rise from zero (its initial value) to the stationary asymptotic value. Conse-

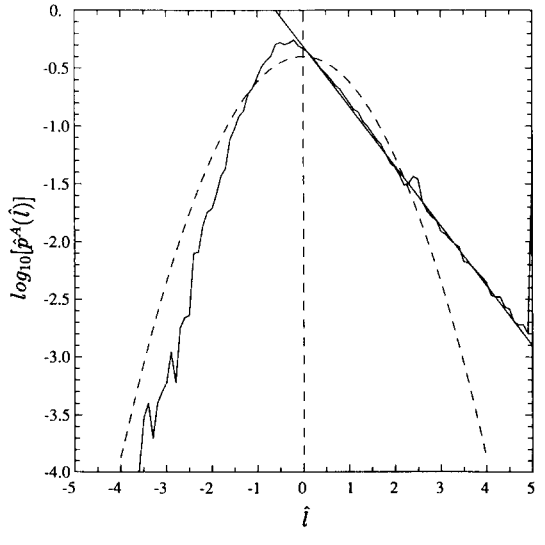

FIG. 5. Standardized area-weighted pdf of $\mathscr{L} = \ln M^*$. Dashed line corresponds to lognormal distribution for M^*: straight line corresponds to $p^A(l) = 0.0172\exp(-0.55l)$.

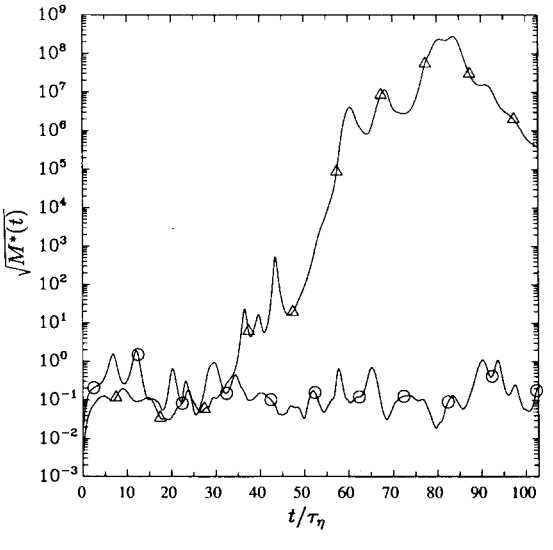

FIG. 6. Normalized root-mean-square curvature against time normalized by the Kolmogorov time scale for a typical element (○), and for the element that attains the greatest curvature (△).

quently, while the distribution is essentially stationary (for $\hat{\mathscr{L}} < 5$, say), nevertheless the mean $\langle M^* \rangle_A$ continually increases, presumably exponentially with time. In view of this behavior, we refer to $\hat{p}^A(\hat{l})$ as being quasistationary.

The occurrence of very small radii of curvatures (e.g., $R \approx 10^{-8}\eta$) raises the question of their significance. If the material surface is used as a model for a layer of small but nonzero thickness δ, then the model most likely breaks down in regions where R/δ is small. Consequently, in this context, radii of curvature much smaller than δ have no significance. But on the other hand if, as here, the fluid is considered to be a continuum, and the mathematical definition of a material surface is used, then there is no lower bound on the values of R that can exist.

We now examine the pdf $p_R^A(r)$ of the normalized mean radius of curvature [Eq. (25)]. [This contains the same information as $p^A(l)$, but emphasizing different features.] The pdf is shown in Fig. 7: the mean $\langle R^* \rangle_A$ is 12.0 and the standard deviation is 12.9. It may be seen that the pdf is almost uniform for $r < 10$. This is consistent with the asymptotic form Eq. (28), which implies (for small r)

$$p_R^A(r) \sim 2\sqrt{2}b(\sqrt{2}r)^{2c-1}, \tag{31}$$

$$\sim 0.051 r^{0.1}. \tag{32}$$

Thus, even though the mean curvature $\langle M^* \rangle_A$ tends to infinity, only about 5% of the surface has a mean radius of curvature R less than the Kolmogorov scale η.

The mean $\langle R \rangle_A$ is quite large: 12 Kolmogorov scales, or a little more than half the integral scale L_1. From this simulation at a single Reynolds number, it is not possible to determine whether $\langle R \rangle_A$, and indeed $p_R^A(r)$, scale with η.

The unweighted pdf of R, $p_R(r)$, is also shown in Fig. 7. It may be seen that there are great differences between the weighted and unweighted pdf's, especially at the origin. The implication is that highly curved elements tend to have less area than more mildly curved elements.

The difference can also be understood in terms of the asymptotic slope c, of the pdf $p^A(l)$ [Eq. (28)]. In Fig. 4, $t'/\tau_\eta = 0$ corresponds to the unweighted pdf, and its asymptotic slope is less than that for the area-weighted pdf ($t'/\tau_\eta = 15.5$). It is evident from Eq. (31) that a slope c less than $\frac{1}{2}$ results in the pdf increasing as r tends to zero.

C. Surface element shape

The shape of the surface at each point is determined by the relative values of the two principal curvatures. We define the shape parameter θ by

$$\theta = k_s/k_l, \tag{33}$$

where k_s and k_l are the smaller and larger of k_1 and k_2 in absolute magnitude.

Possible values of θ lie between -1 and 1. The value $\theta = 1$ corresponds to a spherical element ($k_1 = k_2$); the value $\theta = 0$ corresponds to a cylindrical element ($k_1 = 0$ or $k_2 = 0$); and the value of $\theta = -1$ corresponds to a pseudo-spherical element ($k_1 = -k_2$).

Figure 8 shows the area-weighted pdf of θ, $p_\theta^A(\phi)$. It may be seen that there is a sharp peak at $\theta = 0$ (cylindrical elements), while negative values are more likely than positive ones (Prob $\{\theta < 0\} \approx 0.6$). In particular, the pdf is zero at $\theta = 1$.

The peak at $\theta = 0$ is investigated further in Fig. 9, which shows a contour plot of the unweighted joint pdf of $\mathscr{L} = \ln M^*$ and θ. The ordinate is standardized by the mean $\langle \mathscr{L} \rangle$ and standard deviation σ. (The area-weighted joint pdf is similar in shape but contains too much statistical error to be presented.) It is evident from the figure that the more curved the element, the more nearly is it cylindrical.

To quantify the shape of the highly curved elements, Figs. 10 and 11 show the area-weighted mean and variance of θ conditional on $\mathscr{L} = l$. For $\hat{l}$ greater than unity, the conditional variance decays exponentially as $e^{-0.73l}$, while the conditional mean is essentially zero—certainly much less

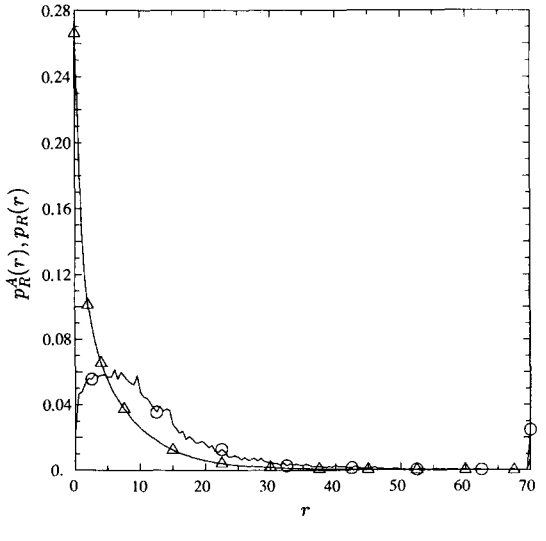

FIG. 7. Area-weighted (○) and unweighted (△) pdf of normalized mean radius of curvature.

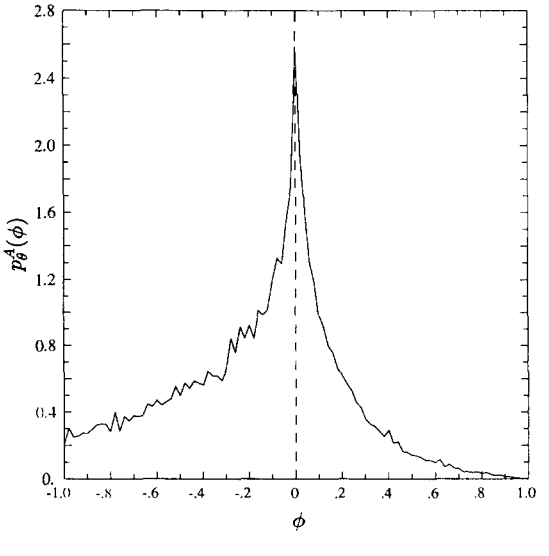

FIG. 8. Area-weighted pdf of the shape parameter θ.

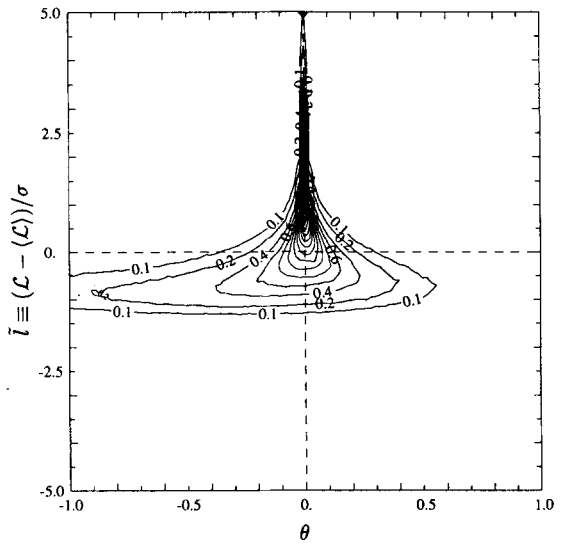

FIG. 9. Contour plot of the (unweighted) joint pdf of $\mathcal{L} = \ln M^*$ and θ.

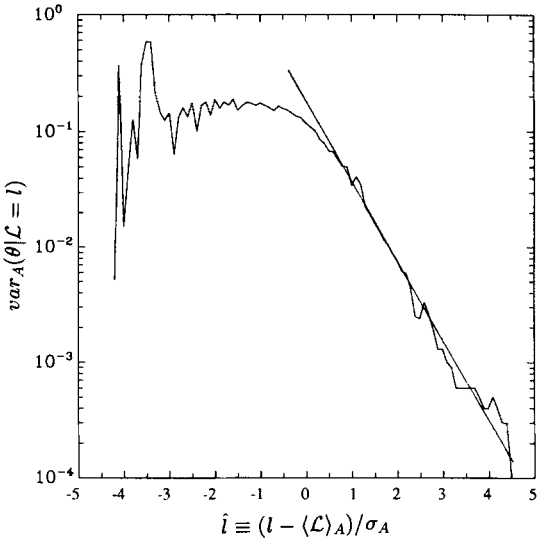

FIG. 11. Area-weighted variance of the shape parameter conditional on mean-square curvature. Straight line corresponds to $\mathrm{var}_A(\theta|\mathcal{L} = l) = 0.0057 \exp(-0.73l)$.

than the conditional standard deviation. Three related observations stem from the observed behavior of the conditional variance.

First, highly curved elements ($R \ll \eta$) might have been expected to have a self-similar distribution of shapes. This is clearly not the case since the variance of the shape parameter θ depends strongly on the curvature $\mathcal{L}$.

Second, although the elements tend to be more closely cylindrical (i.e., $|\theta| = |k_s/k_l|$ decreases) as the mean-square curvature increases, nevertheless the conditional variance of the smaller curvature k_s increases. From the definitions of M^*, $\mathcal{L}$, and θ [Eqs. (20), (21), and (32), respectively] we have

$$(\eta k_s)^2 = 2[\theta^2/(1+\theta^2)]e^{\mathcal{L}}. \tag{34}$$

Hence for large $\mathcal{L}$ (and $\theta^2 \ll 1$) we obtain

$$\langle (\eta k_s)^2 | \mathcal{L} = l \rangle_A = 2\langle \theta^2 | \mathcal{L} = l \rangle_A e^l, \tag{35}$$

$$\sim e^{-0.73l} e^l = e^{0.27l}. \tag{36}$$

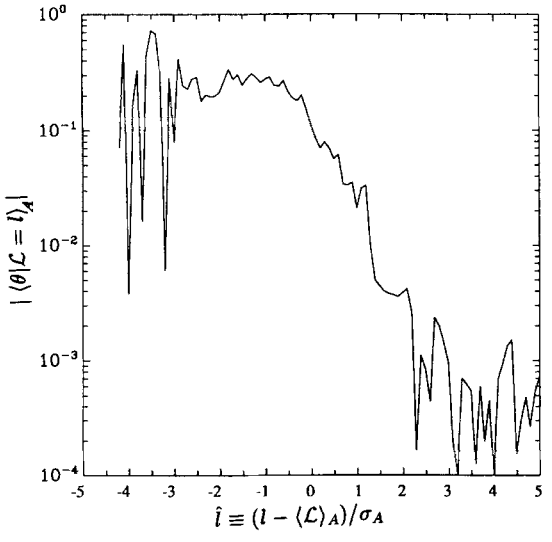

FIG. 10. Area-weighted mean of the shape parameter conditional on mean-square curvature.

Third, the variance of the Gauss curvature K,

$$K^* = K\eta^2 = k_1 k_2 \eta^2, \tag{37}$$

is infinite. From the given definitions, K is related to θ and M^* by

$$K^* = 2\theta M^*/(1+\theta^2). \tag{38}$$

It is curious that although K^* is zero for a cylindrical element, the mean-square $\langle K^{*2} \rangle_A$ is infinite—or,rather, tends to infinity as the surface evolves. From Eq. (38) we have

$$\langle K^{*2} \rangle \geqslant \langle \theta^2 M^{*2} \rangle = \int_{-\infty}^{\infty} \langle \theta^2 | \mathcal{L} = l \rangle e^{2l} p^A(l) dl. \tag{39}$$

Now for large l, the conditional variance decays as $e^{-0.73l}$ and pdf as $e^{-0.55l}$. Evidently these decay rates are insufficient for the integral in Eq. (39) to converge.

V. DISCUSSION AND CONCLUSION

Surface curvature statistics have been obtained from a direct numerical simulation of isotropic turbulence by the method of tracking an ensemble of infinitesimal surface elements. The method allows the accurate calculation of very small radii of curvature—less than a millionth of the Kolmogorov scale η—even though the grid spacing is of order η. The principal numerical error is the statistical error resulting from the finite size (8192) of the ensemble.

The results obtained are different statistics of the principal curvatures, k_1 and k_2. Some care is needed in stating the main results since, superficially, they appear paradoxical. The pdf of $\mathcal{L} = \ln M$ [where $M = \frac{1}{2}(k_1^2 + k_2^2)$ is the mean-square curvature] is essentially statistically stationary after about 15 Kolmogorov time scales: similarly for the pdf of the mean radius of curvature $R \equiv 1/\sqrt{2M}$. The (area-weighted) expectation of R is large compared to the Kolmogorov scale ($\langle R \rangle_A \approx 12\eta$). But for small radii, the pdf of R is approxi-

mately uniform, with about 5% probability of R being less than η.

Although $\langle R \rangle_A$ is large compared to η, the results strongly suggest that $\langle M \rangle_A$ tends to infinity presumably exponentially with time. (The extreme tail of the pdf of ln M is not stationary.)

The shape of the surface elements has been investigated through the shape parameter $\theta = k_s/k_l$, where k_s and k_l are the smaller and larger principal curvatures in absolute magnitude. The pdf of θ is zero for $\theta = 1$, indicating that spherical elements ($k_1 = k_2$) are very improbable. There is a pronounced peak at $\theta = 0$, corresponding to cylindrical elements ($k_1 = 0$ or $k_2 = 0$). It is found that the highly curved elements (large M) are very close to cylindrical. For example, for $M = 50/\eta^2$ (i.e., $R = \eta/10$) the conditional standard deviation of θ is 0.06. (The conditional mean is zero, to within statistical error.)

For an exactly cylindrical element the Gauss curvature $K = k_1 k_2$ is zero. Nevertheless it is found that the expectation $\langle K^2 \rangle_A$ tends to infinity.

From the one-point statistics of curvature it is not possible to deduce the shape of the material surface as a whole. However, the results obtained are consistent with the following conventional picture. Over most of the surface the straining tends to stretch the surface and reduce its wrinkling. For this reason the mean radius of curvature is large ($\langle R \rangle_A \approx 12\eta$). But in particular regions the surface is folded over, and subsequent straining increases the curvature at the fold.

The line of the fold is curved (k_s) much less than curvature of the fold itself (k_l), thus yielding nearly cylindrical surface elements ($k_s/k_l = \theta \approx 0$).

This study leaves open the question of how the pdf of the mean radius of curvature R scales with Reynolds number. The evolution of curvature [Eq. (14)] depends solely on velocity gradients, which, to a first approximation, scale with the Kolmogorov scales. It is reasonable to conjecture, therefore, that R scales with η: that is, that $p_R^A(r)$—the pdf of R/η—is independent of Reynolds number. This conjecture can be tested by a future simulation at a higher Reynolds number.

ACKNOWLEDGMENTS

This paper was written while the first author was a visitor at Cambridge University Engineering Department. The support and encouragement of Professor K. N. C. Bray is gratefully acknowledged.

This work was supported by the U. S. Air Force Office of Scientific Research (Grant No. AFOSR-88-0052). Computations conducted during the research were performed on the Cornell National Supercomputer Facility, which is supported in part by the National Science Foundation, New York State, the IBM Corporation and the members of the Corporate Research Institute.

[1] G. K. Batchelor, Proc. R. Soc. London Ser. A **213**, 349 (1952).
[2] G. K. Batchelor, J. Fluid Mech. **5**, 113 (1959).
[3] N. Peters, in *The 21st International Symposium on Combustion* (The Combustion Institute, Pittsburgh, 1986).
[4] S. B. Pope, Annu. Rev. Fluid Mech. **19**, 237 (1987).
[5] W. J. Cocke, Phys. Fluids **12**, 2488 (1969).
[6] S. A. Orszag, Phys. Fluids **13**, 2203 (1970).
[7] P. K. Yeung, S. S. Girimaji, and S. B. Pope, Combust. Flame (in press).
[8] S. B. Pope, Int. J. Eng. Sci. **26**, 445 (1988).
[9] M. P. Do Carmo, *Differential Geometry of Curves and Surfaces* (Prentice–Hall, Englewood Cliffs, NJ, 1976).
[10] B. B. Mandlebrot, J. Fluid Mech. **72**, 401 (1975).
[11] F. C. Gouldin, Combust. Flame **68**, 249 (1987).
[12] F. A. Williams, *Combustion Theory* (Benjamin, New York, 1985).
[13] S. Osher and J. A. Sethian, J. Comput. Phys. **79**, 12 (1988).
[14] R. S. Rogallo, NASA Tech. Memo 81315, (1981).
[15] V. Eswaran and S. B. Pope, Comput. Fluids **16**, 257 (1988).
[16] P. K. Yeung and S. B. Pope, J. Fluid Mech. **207**, 531 (1989).
[17] P. K. Yeung and S. B. Pope, J. Comput. Phys. **79**, 373 (1988).